Theoretical Studies on the CH_3CO + Cl Reaction: Hydrogen Abstraction versus CO Displacement

Raman Sumathi* and Minh Tho Nguyen*

Department of Chemistry, University of Leuven, Celestijnenlaan 200F, B-3001 Leuven, Belgium

Received: February 26, 1998; In Final Form: June 23, 1998

The geometries, energies, and vibrational frequencies of the reactants, transition structures, intermediates, and products of the reaction of the acetyl radical with atomic chlorine have been determined by ab initio molecular orbital theory at the second-order Møller Plesset perturbation (MP2) level. Energies have been recalculated at the quadratic configuration interaction QCISD(T) level by using geometries obtained at MP2 level. The energy of the initial acetyl chloride adduct CH_3COCl (**1**), formed by barrier-free combination, lies 78 kcal/mol below the reactants. Two major reaction routes are open to the chemically activated adduct **1**: molecular dissociation to $H_2C{=}C{=}O$ + HCl (**3**), and the secondary formation of ketene via 1-chlorovinyl alcohol (**2**). Both these processes are energetically feasible to the thermal reactants and should hence lead to a spontaneous emission of a vibrationally hot HCl molecule as observed by Maricq et al. (Int. J. Chem. Kinet. **1997**, *29*, 421). The thermodynamically most stable products, CH_3Cl + CO, should preferably be formed via direct displacement of CO from CH_3CO by Cl; this reaction proceeds via a loose complex between $Cl^{\delta-}$ and $CH_3CO^{\delta+}$, which explains the delayed emission of CO in the diode laser study of the Cl + CH_3CO reaction. The energy barrier for decarbonylation of the adduct **1** is quite high and thereby is not accessible to the thermal reactants. The present potential energy surface reveals this reaction to be a capture-limited association−elimination reaction with a very high and pressure-independent rate coefficient.

Introduction

Photolysis of molecular chlorine in the presence of a hydrocarbon readily leads to the formation of the chain-propagating organic hydrocarbon radicals via the following reaction:

$$Cl + RH \rightarrow R\cdot + HCl$$

whose properties and chemistry are of importance in combusion, atmospheric, and interstellar processes. Consequently, there is a growing literature of studies on the kinetics of the reactions of chlorine atoms with hydrocarbon molecules and other propagating reactions in a radical chain mechanism.[1,2] Equally important are the chain-terminating reactions below, which measure the efficiency of a chain reaction.

$$R + R \rightarrow \text{products}$$

$$R + Cl \rightarrow \text{products}$$

Recently Maricq et al.[1] reported the real-time kinetic measurements for one such chain-terminating reaction, namely, Cl + CH_3CO. They investigated the reaction over a pressure range of 10−200 Torr and a temperature range of 215−353 K and reported its rate constant value to be $(1.8 \pm 0.5) \times 10^{-10}$ cm^3 s^{-1}. From their experiments, the authors identified ketene H_2CCO as a product but could not differentiate between an addition−elimination mechanism, viz., CH_3COCl formation followed by the four-centered elimination of HCl, and a direct abstraction of hydrogen by Cl from CH_3CO. Three of their observations deserve more attention: (1). There was no pressure dependence on the ketene H_2CCO formation rate constant in the range 10−200 Torr, which is consistent with an addition−elimination mechanism. In our earlier work[3] on acetyl chloride at the Møller Plesset perturbation (MP2)/6−31G*//HF/6−31G* level, we found the energy for the four-membered transition state for the 1,2-elimination of HCl was ∼33 kcal/mol below the reactant limit, Cl+ CH_3CO. Hence, the acetyl chloride adduct, once formed, is expected to undergo a rapid unimolecular dissociation to HCl and ketene. (2) The distinct delay in CO formation relative to that of the ketene limited the reaction producing CH_3Cl + CO to <10%. This observation, in combination with our earlier potential energy surface,[3] is also consistent with an addition−elimination mechanism since the saddle point for the 1,1-elimination of CO lies energetically above (∼19 kcal/mol) the reactant limit. (3) The time dependence of the IR absorption profile of CH_2CO did not show any difference when the buffer gas was changed from N_2 to C_2F_6, which means that the ketene product was not vibrationally excited.

This last observation is in contrast to our expectations from the structure of the transition state for HCl elimination, which indicates that both the ketene and HCl are not fully formed[3] and hence should be to a large extent vibrationally excited. Moreover, for the HX elimination from haloethanes,[4] 50−60% of the available energy is released to the internal energy of the alkene product. Hence, a sizable amount of ketene might be formed via direct hydrogen abstraction. However, as discussed by Rowland and Hess,[5] the direct displacement of CO by Cl to form CH_3Cl would be quite plausible and more favored over the direct hydrogen abstraction because the C−C bond in the

* Author for correspondence. FAX: 32-16-327992. E-mail: minh.nguyen@chem.kuleuven.ac.be.

S1089-5639(98)01312-7 CCC: $15.00
Published on Web 09/25/1998

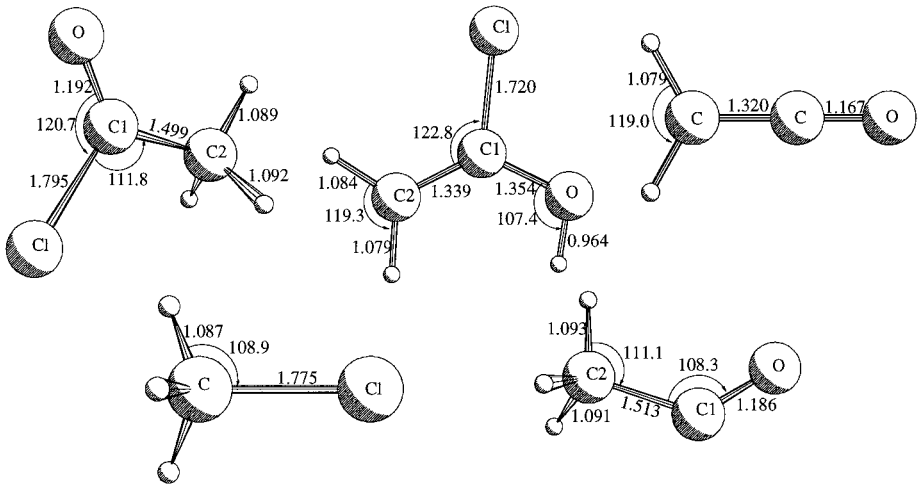

Figure 1. MP2/6−311++G(d,p)-optimized geometries of the intermediates and products of the $CH_3CO\cdot$ + Cl· reaction. Bond lengths are given in Å and bond angles in degrees. **1**, CH_3COCl; **2**, $H_2C{=}C(OH)Cl$; **3**, $H_2C{=}C{=}O$ + HCl; **4**, CH_3Cl + CO; **5**, CH_3CO + Cl.

acetyl radical (11.4 kcal/mol)[6] is much weaker than the C−H bond (42 kcal/mol).[7] Also, the reaction enthalpy for the formation of CH_3Cl + CO from CH_3COCl is +12.2 kcal/mol, which is less endothermic than that for H_2CCO + HCl at +25 kcal/mol.[8] Although such a CO-displacement reaction to form CH_3Cl should be favored on thermodynamic grounds, it was not observed by Maricq et al.[1] Consequently, these observations are somewhat puzzling and call for a thorough investigation on the direct hydrogen abstraction/displacement channels.

Whereas the analogous Cl + C_2H_5 reaction was established by Seakins et al.[9] to proceed via an addition−elimination mechanism from the nascent HCl vibrational distributions, the Cl + CH_3O_2 reaction proceeds via two channels to give approximately equal yields of ClO and HCl, an observation consistent with an adduct formation followed by a rapid rearrangement to two sets of products. In addition, from a mechanistic viewpoint, a displacement of a closed-shell CO fragment by the atomic Cl· radical is intriguing. Up to now, theoretical and experimental studies[1,10−13] have mainly been focused on the gas-phase and condensed-phase unimolecular thermal and photochemical dissociations of acetyl chloride from its S_0,[1] S_1,[10−13] and T_1[1] potential energy surfaces. As a first step toward understanding the CH_3CO + Cl reaction kinetics, we have reexplored the singlet ground-state potential energy surface, including the missing portions, by using higher-level calculations. In our earlier publication[3] we did not consider the crucial direct hydrogen abstraction, direct displacement of CO by Cl·, or the reactions leading to and arising from the 1-chlorovinyl alcohol intermediate. Our primary aim in the present investigation is to identify the saddle points for these important channels and in turn to gain some additional insights into the reaction kinetics.

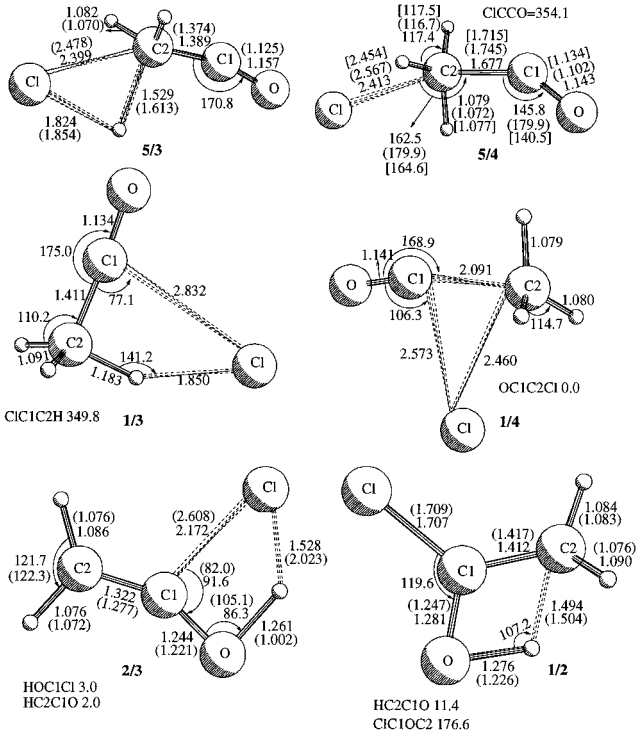

Figure 2. MP2/6−311++G(d,p)-optimized geometries of the transition structures **1**/**3**, **1**/**4**, **5**/**3**, **5**/**4**, **1**/**2**, and **2**/**3** relevant to the $CH_3CO\cdot$ + Cl· potential energy surface. Numbers in parentheses and brackets refer to HF/6−31G(d,p) and B3LYP/6−311++G(d,p) values, respectively. Bond lengths are given in Å and bond angles in degrees.

Computational Details

All calculations were performed with the GAUSSIAN 94 program.[14] Geometries of reactants, adducts, and transition states were optimized at the (U)MP2/6−311++G(d,p) level by using analytical gradient methods. All electrons were included for the calculation of correlation energy. We note that, as a measure of the UHF spin contamination, the expectation value of the $\langle S^2 \rangle$ operator was not much greater than 0.75 for doublets. Harmonic vibrational frequencies were calculated at the (U)-MP2/6−311++G(d,p) level to characterize the nature of the stationary points on the potential energy surface. Single-point electronic energy calculations, made by using the quadratic configuration interaction singles and doubles substitution with triples corrections, were subsequently performed on all relevant stationary points with the 6−311++G(d,p) basis set, QCISD-(T)/6−311++G(d,p)//MP2/6−311++G(d,p), with use of the optimized MP2 geometries. In particular, the transition structure between **1** and **3**, (**1**/**3**) has been optimized at Hartree−Fock (HF), MP2, MP3, MP4(SDQ), CISD, QCISD, and B3LYP-DFT levels by using the 6−31G(d,p) basis set to establish the degree of looseness of this transition state. In the MP3, MP4(SDQ), CISD, and QCISD calculations, only valence electrons were taken into account in evaluating of the correlation energy, and the transition-state geometry was optimized by using analytical

TABLE 1: Unscaled Harmonic Vibrational Frequencies (in cm^{-1}) and Rotational Constants (in GHz) of the Various Isomers and Saddle Points on $CH_3CO\cdot + Cl\cdot$ Potential Energy Surface

1	2	1/2	1/3	1/4	2/3	5/3[a]	5/4
138.8	258.4	2265.4i	741.2i	819.8i	1910.2i	1236.9i	687.0i
352.3	390.6	363.8	150.0	190.9	100.7	150.6	33.2
458.5	448.7	466.2	182.7	66.2	258.1	410.2	97.9
522.3	505.6	529.7	349.0	184.2	455.3	418.4	304.4
625.9	659.7	615.7	413.0	262.2	487.8	533.9	350.2
983.1	694.8	773.4	817.7	375.2	574.6	556.6	442.3
1046.7	716.5	830.6	990.1	781.5	587.9	879.3	898.0
1139.1	980.7	1063.1	1062.6	858.0	686.2	1045.2	1069.7
1406.2	1161.0	1161.9	1146.0	1266.6	960.8	1067.1	1144.0
1481.4	1350.1	1302.5	1366.0	1433.5	1130.1	1117.4	1369.9
1482.2	1442.3	1479.6	1423.1	1499.5	1408.9	1201.1	1398.6
1848.3	1691.9	1538.4	1987.7	2085.7	1666.4	1338.6	2054.7
3102.0	3211.9	1952.3	2297.0	3178.4	1969.5	2138.5	3127.4
3195.6	3330.7	3161.6	3135.1	3327.7	3206.9	3205.2	3296.9
3220.2	3855.1	3270.9	3226.1	3359.0	3356.5	3316.4	3351.6
10.109	10.592	12.285	9.940	7.468	10.578	53.819	48.335
4.953	5.163	4.704	3.123	3.879	4.384	1.704	1.541
3.394	3.471	3.449	2.414	2.597	3.100	1.670	1.509

[a] Corresponding to a constrained optimization (see text).

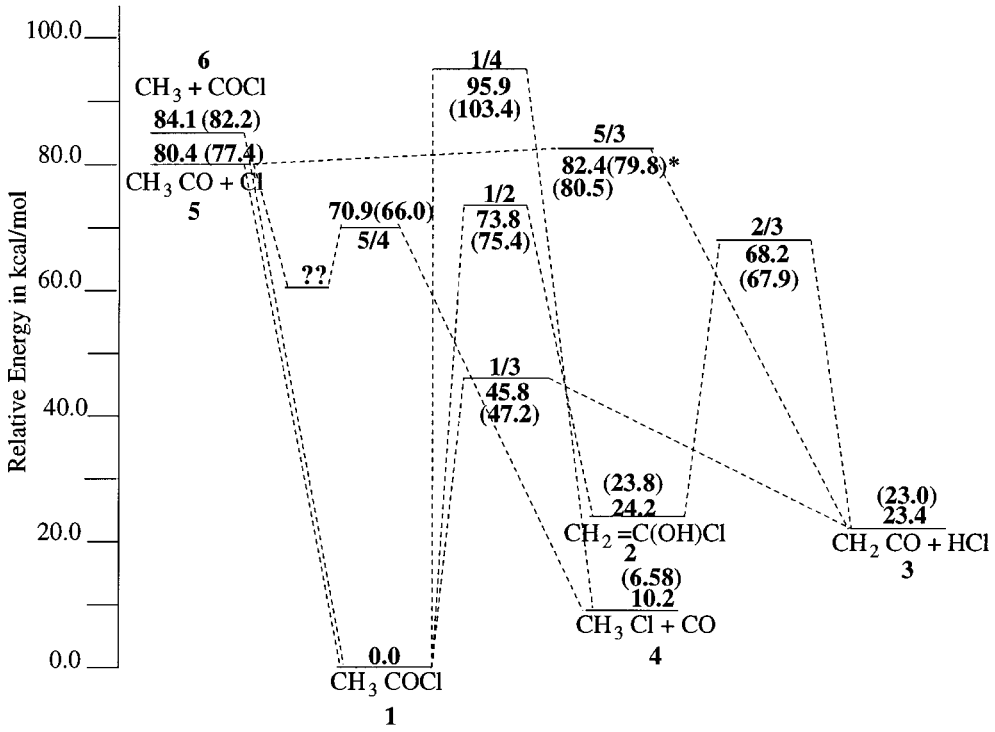

Figure 3. The overall profile of potential energy surface related to the $CH_3CO\cdot + Cl\cdot$ reaction calculated at MP2/6−311++G(d,p) + zero-point vibrational energies (ZPE) level of theory. Numbers in parentheses correspond to QCISD(T)/6−311++G(d,p)//MP2/6−311++G(d,p) values corrected for ZPE by using MP2/6−311++G(d,p) frequencies. * represents ZPE-uncorrected values.

gradient methods. Intrinsic reaction coordinate (IRC) calculations[15] were performed to follow the minimum energy path from the transition-state structure to the reactant as well as to the product.

Results and Discussion

The MP2/6−311++G(d,p)-optimized geometries of the intermediates, viz., acetyl chloride (**1**), 1-chlorovinyl alcohol (**2**), acetyl radical, and the reaction products, are shown in Figure 1. The transition structures are numbered with both the reactant and product numbers. The geometries of the saddle points for the direct hydrogen abstraction (**5**/**3**), the addition−elimination channel leading to CH_2CO + HCl (**1**/**3**), CO displacement (**5**/**4**), and the addition−elimination pathway for CH_3Cl + CO (**1**/**4**) are shown in Figure 2. The transition structures for the rearrangement to 1-chlorovinyl alcohol (**1**/**2**) and for the secondary elimination of HX from $CH_2C(OH)Cl$ (**2**/**3**) are also shown in Figure 2. The numbers in parentheses refer to the optimized values at the HF/6−31G(d,p) level, where applicable. A schematic representation of the potential energy surface for the CH_3CO + Cl reaction is shown in Figure 3. The numbers displayed in parentheses correspond to QCISD(T)/6−311++G(d,p)//MP2/6−311++G(d,p) values corrected for zero-point energies by using MP2/6−311++G(d,p) frequencies. These represent our best estimates for relative energies and will hence be used in the following discussion. The harmonic vibrational frequencies of the transition structures are listed in Table 1,

TABLE 2: Optimized Geometrical Parameters of the Transition Structure 1/3 at Different Levels of Calculation

parameter[a]	HF	MP2	MP3	MP4	CISD	QCISD	DFT	MP2[b]	DFT[c]
				Bond lengths, Å					
H....Cl	1.813	1.891	1.859	1.855	1.862	1.855	1.857	1.850	1.866
C1....Cl	3.285	2.953	2.931	2.949	3.014	2.955	2.894	2.932	2.887
C2−H1	1.200	1.178	1.175	1.178	1.171	1.178	1.193	1.183	1.189
C1−C2	1.411	1.408	1.419	1.421	1.415	1.422	1.408	1.411	1.398
C1−O	1.105	1.145	1.126	1.139	1.122	1.137	1.139	1.134	1.126
C2−H2	1.082	1.092	1.086	1.087	1.083	1.088	1.094	1.091	1.091
				Bond angles, °					
C2−C1−O1	176.0	179.8	179.0	179.7	178.9	179.7	174.6	175.0	173.5
C2−H1−C1	163.2	146.6	147.4	148.2	150.7	148.2	143.2	141.2	140.5
H1−Cl−C1	32.1	40.3	40.6	40.3	38.7	40.3	42.3	42.3	41.9
Cl−C1−C2	65.2	75.8	75.4	74.9	73.3	74.7	76.2	77.1	75.8
C1−C2−H1	99.5	97.2	96.6	96.6	97.3	96.8	98.2	95.3	97.3
H2−C2−H3	113.9	113.3	113.5	113.4	113.6	113.4	112.7	119.2	113.2

[a] Determined with the 6−31G(d,p) basis set unless otherwise stated. [b] Corresponding to the MP2(FU)/6−311++G(d,p) level of optimization. [c] Corresponding to the B3LYP/6−311++G(3df,2p) level of optimization.

TABLE 3: Calculated QCISD(T)/6−311++G(d,p) Total Energies and Zero-Point Energies (ZPE) for Species Involved in the $CH_3CO\cdot$ + Cl·

species	total energy, au[a]	ZPE, kcal/mol[b]
$CH_3CO\cdot$	−152.847638	27.5
Cl·	−459.604463	
CH_3COCl (**1**)	−612.579449	30.0
CH_2=C(OH)Cl (**2**)	−612.540822	29.6
CH_3Cl	−499.467121	24.2
CO	−113.097409	3.0
CH_2CO	−152.268959	19.7
HCl	−460.264434	4.4
1/2	−612.453628	26.5
1/3	−612.498615	26.5
1/4	−612.409309	26.7
2/3	−612.461815	24.1
5/3[c]	−612.442897	24.8
5/4	−612.470160	27.1

[a] Based on optimized geometries at the MP2/6−311++G(d,p) level. [b] Zero-point energies determined for unscaled frequencies at MP2/6−311++G(d,p) level. [c] Corresponding to a constrained optimization (see text).

along with their rotational constants. The optimized geometrical parameters of the transition structure **1/3** at different levels of calculation are collected in Table 2. The QCISD(T) energies of the various stationary points are tabulated in Table 3 along with their zero-point vibrational energies. The pathways for the molecular elimination of HCl from acetyl chloride and the direct displacement of CO by Cl are summarized in the data presented as Supporting Information (as Tables 4 and 5).

As mentioned in the Introduction, the reaction could proceed via (1) the addition of the radical centers to form the C−Cl bond

$$CH_3CO\cdot + Cl\cdot\ \mathbf{5} \rightarrow CH_3COCl\ \mathbf{1} \qquad (1)$$

and (or) (2) by the attack of Cl· to one of the three hydrogens of the CH_3 moiety of acetyl radical

$$CH_3CO\cdot + Cl\cdot\ \mathbf{5} \rightarrow HCl + CH_2CO\ \mathbf{3} \qquad (2)$$

and (or) (3) by the attack of Cl· to the carbon of the methyl group leading to the displacement of CO.

$$CH_3CO\cdot + Cl\cdot\ \mathbf{5} \rightarrow CH_3Cl + CO\ \mathbf{4} \qquad (3)$$

The attack of Cl· at the carbonyl carbon of $CH_3CO\cdot$, where a major fraction of the radical electron density resides, leads to the covalently bonded stable CH_3COCl **1** intermediate. Because this process involves a bond formation between two radical centers, it is a barrierless association and hence is expected to be fast and to play a significant role in the reaction kinetics. The adduct **1** is stabilized by 77.4 kcal/mol with respect to the reactant radicals, $CH_3CO\cdot$ + Cl·. However, the experimental C−Cl bond energy D_0(C−Cl) in acetyl chloride has been evaluated[16] to be 83 ± 1 kcal/mol. The difference probably arises from the relatively small size of the basis set and the application of the single configuration treatment. Our aim in this work however, was to obtain an overall understanding about the potential energy surface at a reasonable and computationally feasible level of calculation.

The various possible dissociation and isomerization reactions from the energized adduct, CH_3COCl (**1**), are

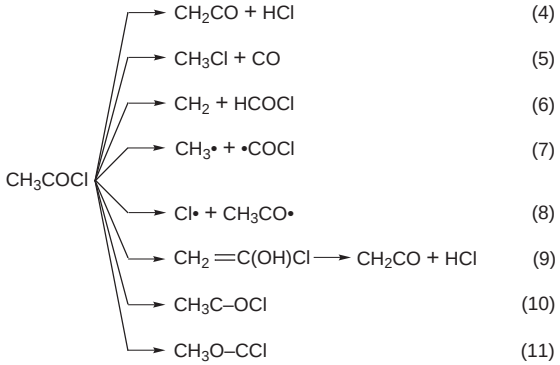

Our earlier investigation[3] at MP2/6−31G*//HF/6−31G* level showed that the above reactions 6, 10, and 11 require very high energy barriers, virtually above the C−C (reaction 7) and C−Cl (reaction 8) bond dissociation limits, and hence are of less importance in the unimolecular dissociation dynamics of acetyl chloride. In addition, the corresponding reactions in CH_2FCOCl also have a very high barrier, even at a higher level of calculation,[17] the MP2(FU)/6−311++G(d,p) level. Hence, we have not considered these reactions for the present investigation and will not discuss them further. We have focused on the remaining reactions and determined their improved activation barriers at a reasonably higher level of calculation. Since direct hydrogen abstraction is associated with simultaneous formation of a H−Cl bond and cleavage of a C−H bond, but the bond strengths of H−Cl and C−H bonds are different, one would expect this path to face a barrier. Similarly, the CO displacement, if any, will also be associated with an energy barrier.

Formation of Ketene and Hydrogen Chloride. *From the acetyl chloride adduct (reaction 4):* As shown in Figure 3, the

most favorable dissociation channel is a 1,2-elimination of HCl along with the formation of ketene, CH_2CO. The calculated transition structure for this dissociation is given in Table 2 at different levels of correlation treatment with a 6−31G(d,p) basis set. As seen in Figure 2, this transition structure is very loose with an elongated C−Cl bond. Optimization of this saddle point has in fact been carried out at different levels to establish the degree of looseness in this four-membered transition structure, which is a long-disputed and debated factor in the study of HX elimination from haloalkanes.[18] The four bond lengths of the four membered transition state, viz., the dissociating C−H and C−Cl bonds, and the forming H−Cl and the olefinic C−C bonds determine a quadrilateral geometry of the four atoms. The Cl−C1−C2 bond angle decreases from approximately tetrahedral in the reactant to slightly less than 90° in the transition state, and the sum of Cl−C1−C2 and C1−C2−H1 bond angles at all levels of calculation is approximately equal to 170°. Overall, this transition-state structure turns out to be very similar to the ones observed for HX elimination from alkyl halides.[18] A careful look at Table 2 reveals that the geometrical parameters obtained in different calculations are, to a good approximation, very nearly the same, differing only between the results at the HF and correlated levels. In particular, the dissociating C−Cl bond length at the HF level is ∼0.4 Å larger than that predicted by other correlation methods, and the forming Cl−H bond is 0.05 Å shorter. Also, from Table 2 the results at MP2(FU)/6−311++G(d,p) and B3LYP/6−311++G(3df,-2p) levels in Table 2, the basis set obviously does not have much influence on the geometry of this transition state. The C1−C2 bond length is between the single bond in acetyl chloride (1.499 Å) and the double bond in the ketene (1.320 Å). This qualitatively suggests a vibrationally excited ketene in addition to a vibrationally hot HCl species, in contrast to the experimental observations.

The C−O bond length in **1**/**3** (1.134 Å) is surprisingly smaller than that in the reactant $CH_3CO\cdot$ (1.186 Å), in the adduct CH_3-COCl (1.192 Å) and in the ketene product (1.167 Å), too. In reality, such a short bond length corresponds to C ≡ O system (1.139 Å) and in the transition structure, since the C−C−O bond angle is ∼175°, the carbonyl carbon has achieved an sp-hybridization and it exists as $CH_3CO^{\delta+}Cl^{\delta-}$. Examination of the Mulliken atomic charges reveals a −0.66e charge on the chlorine, +0.77e on the carbonyl carbon, −0.19e on the oxygen, and just +0.07e on the methyl carbon. Thus, the magnitude of the positive charge on the methyl carbon is substantially smaller than the positive charge on the C1. In other words, the C2−H bond has a covalent character, while the C1−Cl bond has a semiionic character. The main difference in the structure of **1**/**3** between HF and correlated methods is probably related to the larger polarization of charges at the HF level: Cl (−0.72e), C (0.72e), O (−0.25e), and the methyl carbon (0.25e). Indeed, it leads to an asymmetric model of the transition structure akin to the one proposed by Toto et al.[18] for the HX elimination from haloalkanes. The C−X and H−X bonds are almost completely broken. Beyond the transition structure, the reaction involves lengthening of the C−H bond along with a redistribution of charge in the $CH_3CO^{\delta+}$ fragment. It is tempting to suggest that such a charge separation or redistribution in the transition structure is responsible for the experimentally observed vibrationally cold ketene product.

Yet another pathway for the ketene formation starting from **1** could be rationalized in terms of a two-step process involving the 1-chlorovinyl alcohol intermediate **2**. Such a process plays a major role in the thermal decomposition of acetic acid[19] but a minor role in that of acetyl cyanide.[20] Transition-structure searches for 1,3-hydrogen migration from carbon to oxygen located a four-membered transition state **1**/**2** with all four atoms lying approximately in the same plane. The migrating hydrogen is 1.49 and 1.28 Å from the migrating origin and terminus, respectively. The reaction coordinate has been identified as the asymmetric C···H−O stretch, and the magnitude of the imaginary vibration in the transition state equals 1910i cm^{-1}. The transition structure **1**/**2** lies below the thermal reactant limit and hence is expected to contribute the reaction kinetics. Because the barrier for this process is ∼28 kcal/mol above that for **1**/**3**, the percentage contribution of reaction 9 toward ketene formation will be quite low. Once formed, however, **2** will undergo 1,2-elimination of HCl spontaneously since the barrier for this process is lower than the excess energy that is available to **2**. Nevertheless, owing to the decrease in the reaction probability with the increasing number of reaction intermediates and as well to the higher barrier height for the first step (**1** → **2**), we expect the percentage contribution of this channel toward the ketene formation to be low. Thus, the principal pathways leading to ketene and HCl via **1** are as follows: the former being favored

$$CH_3CO\cdot + Cl\cdot \rightarrow \mathbf{1} \xrightarrow{1/3} \mathbf{3}$$

$$CH_3CO\cdot + Cl\cdot \rightarrow \mathbf{1} \xrightarrow{1/2} \mathbf{2} \xrightarrow{2/3} \mathbf{3}$$

over the latter at ordinary temperatures and pressures. At high pressures, conversion of acetyl chloride to chlorovinyl alcohol will be less important than its dissociation into CH_2CO + HCl and (or) its stabilization. Hence at high pressures the ketene formation would occur entirely through the former pathway.

Via direct hydrogen abstraction (reaction 2): The direct hydrogen abstraction reaction is exoergic and, according to Hammond's postulate, the transition state should be more reactant-like than product-like. Hence, transition-state searches were performed, starting from a 90° and a 180° approach of the chlorine atom to one of the three hydrogens of CH_3 in a trans orientation with respect to carbonyl carbon ($\tau_{Cl-H1-C1-C2}$ = 180°). In the former case, all our attempts invariably lead to the transition structure **1**/**3**, accompanied by the complete 180° rotation of the chlorine atom. When the chlorine atom is approached linearly (Cl−H1−C1 = 180°), it leads to a transition structure for the torsional motion, $\tau_{C2-C1-H1-Cl}$ in the loose O═C2═H_2C1.....H1−Cl van der Waals complex.[21] Consequently, the transition structure **5**/**3** was obtained via a constrained parameter (Cl−H1−C1 = 90°). Analysis of the eigenvector corresponding to the negative eigenvalue of the force constant matrix, 0.78 R_{C-H} − 0.59 R_{H-Cl}, characterizes it as a transition structure for the direct hydrogen abstraction, and the magnitude of the imaginary frequency equals 1237 i cm^{-1}. Though it is not advisable to put any weightage on its structure and energetics, the bond distances for C1−C2 (0.07 Å longer than that in the free ketene) and H−Cl (0.6 Å longer than that in free HCl) in the **5**/**3** adumbrate vibrationally excited HCl as the product. Nevertheless, the partial optimization of **5**/**3** clearly obfuscates the conclusion that part of the ketene is actually formed via direct hydrogen abstraction.

Formation of Carbon Monoxide and Methyl Chloride. *Direct displacement reaction: (reaction 3):* The most interesting and unique transition structure we investigated in this study is **5**/**4**. As it is obvious, reaction 3 correlates two radicals on one side with two neutral molecules on the other side. The corresponding transition structure **5**/**4** has an approximate trigonal bipyramidal geometry. All three hydrogens and the

methyl carbon lie more or less in one plane (HHHC = 16°), and the approaching Cl radical and the detaching CO moiety are in a perpendicular plane. The structure of **5**/**4** is akin to a second-order nucleophilic substitution (S_N2) transition state wherein the incoming nucleophile (Nu^-) forms a bond with one lobe of the p-orbital while the leaving group overlaps with the other lobe of the p-orbital. The C−C and C−Cl bond distances of 1.677 and 2.413 Å, respectively, are indicative of incomplete bond cleavage and bond formation. The C−O distance of 1.143 Å in the transition structure **5**/**4** suggests the formation of a vibrationally cold CO molecule. The C−C−O fragment is not linear and hence would lead to rotational excitation of the CO moiety when the C−C bond is cut off. The transition vector has been identified from the normal-mode eigenvector corresponding to the negative eigenvalue of the force constant matrix as

$$0.69\ R_{C-C} - 0.43\ R_{C-Cl} + 0.25\ \theta_{C-C-O} + 0.40\ \theta_{Cl-C-H}$$

The transition structure **5**/**4** has been optimized at HF/6−31G(d,p), MP2(FU)/6−311++G(d,p), and B3LYP/6−311++G(d,p) levels. As shown in Figure 2, the optimized parameters at the HF level differ from those at the MP2 and B3LYP levels, whereas the geometry obtained at the latter two levels are fairly close to each other. However, the magnitudes of the imaginary frequency—598i (HF), 687i (MP2(FU)), and 571i (B3LYP) cm^{-1}—and the reaction coordinate are similar. At the HF level, the barrier for this process is 10.7 kcal/mol relative to the reactants $CH_3CO\cdot$ + Cl·, whereas at the MP2, QCISD(T), and DFT levels, **5**/**4** is energetically disposed at 9.5, 11.3, and 18.0 kcal/mol, respectively, below the reactants. This suggests an initial formation of a strong complex between $CH_3CO\cdot$ and Cl·, followed by displacement of CO. The Mulliken atomic charges derived from the MP2 wave function at different centers of **5**/**4** are Cl (−0.38e), carbonyl carbon (0.12e), and methyl carbon (0.25e). At HF level, the transition structure is more ionic, as revealed by the Mulliken atomic charges: Cl(−0.81e), carbonyl carbon (0.53e), methyl carbon (0.50e), and carbonyl oxygen (−0.23e). The incoming chlorine atom induces polarization of charge densities in the acetyl fragment. This could suggest a Cl^- + CH_3CO^+ limit. However, the energy of such ionic reactants limit is still higher than the radical limit and hence **5**/**4** cannot correlate to $CH_3CO^+ + Cl^-$ reactants. A Cl.....CH_3-CO structure (not shown) having a C_{3v} symmetry has been found and characterized by two imaginary frequencies. Removal of the symmetry constraint relaxes the geometry of the supersystem to the HCl....H_2CCO complex.[21]

The pathway for the direct displacement of CO by Cl is summarized in Table 3. These data were obtained by following the IRC calculation from **5**/**4** back to the reactant and forward to the products. The data presented here were determined at the B3LYP/6−311++G(d,p) level to reduce the computational effort but still present a good qualitative picture of the energetic and geometric changes occurring during the unimolecular decomposition. As shown in Table 3, the dominant changes as the molecule proceeds from the reactant to its product are represented by the lengthening of the C−C bond in conjunction with a decrease in the C−Cl bond length. Also the C—C—O angle widens and the H—C—C angle simultaneously narrows. Concurrently, the C−O and C−H bond lengths shorten, somewhat, and the Cl—C—C angle first contracts and then recovers its ground-state value. The product molecules, CH_3-Cl and CO, are oriented such that the carbon of the CO is linear with the carbon of the CH_3Cl (Cl—C—C = 177°). The structure of a point close to the reactant complex, according to the IRC calculation, has an atomic charge of 0.64e on the methyl carbon, −0.62e on the chlorine, 0.04e on the carbonyl carbon, and −0.06e on the oxygen. Frequency calculations for this structure characterize it as a saddle point with respect to the Cl−C−C angle. Nevertheless, complete optimization of the structure leads again to the van der Waals complex[21] between HCl and H_2CCO.

Despite this fact, we hesitate to make a link between the van der Waals complex and **4** through **5**/**4**. The reason we failed to find a complex between both radicals Cl· and $CH_3CO\cdot$ is probably the biradical and (or) ionic character of the complex. If such a biradical complex exists, it cannot obviously be treated by the single-reference ab initio methods used in this work. Unfortunately, an appropriate multireference study needed on such a system is at present beyond our computational resources. In view of its unique character in reaction mechanisms, the path **5** → **5**/**4** → **4** deserves a further study by its own. Here, we assume that there is actually a complex lying between **5** and **5**/**4** (that is the sense of the question marks included in Figure 3).

From the acetyl chloride adduct: Decarbonylation transition structure **1**/**4**, as shown in Figure 2, maintains a C_s symmetry. The C−C (2.091 Å) and C−Cl (2.573 Å) distances in this loose three-membered structure are indeed very long, relative to the corresponding distances in the adduct (1.499 and 1.795 Å, respectively). The C═O distance of 1.141 Å is closer to its value in the product carbon monoxide and hence is expected to give rise to the vibrationally cold CO product. Subsequently, the large C(CH_3)—Cl distance of 2.460 Å in **1**/**4** suggests the formation of a vibrationally excited CH_3Cl molecule. However, the barrier for this process is quite high from the adduct (103.4 kcal/mol), and **1**/**4** lies 26 kcal/mol above the initial reactant limit. Hence, this process is apparently not available to the thermal reactants and begins to participate only at higher temperatures.

To summarize, the thermal reactants CH_3CO + Cl lead to formation of the energized CH_3COCl (**1**), which in turn undergoes molecular elimination, yielding vibrationally excited HCl. Also, a fraction of ketene results from the secondary elimination reaction via 1-chlorovinyl alcohol (**2**) as an intermediate. The above two routes account for the fast, direct process because all the transition states in these routes are energetically accessible for the thermal CH_3CO + Cl reactants and are favored over redissociation to CH_3CO + Cl. This establishes the experimental observation that the rate coefficient of CH_3CO + Cl reaction is pressure-independent.

Conclusions

Electronic structure calculations have been used to characterize the reaction between $CH_3CO\cdot$ and Cl· on the lowest singlet potential-energy surface. While geometries and vibrational frequencies for stationary points on the potential energy surface are determined with the UMP2 level of theory and use of the 6−311++G(d,p) basis set, the energies are obtained from QCISD(T) calculations. The main features of the reaction surface are as follows:

• Combination of the reactants $CH_3CO\cdot$ + Cl· to form CH_3-COCl occurs without barrier. On the other hand, the direct hydrogen abstraction (reaction 2) and CO displacement (reaction 3) channels face a barrier. The exact magnitude of their barrier heights, however, could not be established because of an obfuscating transition structure, **5**/**4**. We also could not locate a fully optimized transition structure for direct hydrogen abstraction.

• Two distinct pathways involving dissociation/isomerization are energetically open to the chemically activated initial intermediates, **1** and **2**. The above establishes $CH_3CO\cdot + Cl\cdot$ as a fast and pressure-independent association−elimination reaction, in agreement with the experimental observation.

• At ambient and moderately high temperatures, the dominant reaction channels are (1) the molecular dissociation of CH_3COCl (**1**) to $H_2CCO + HCl$ (**3**), and (2) the competing isomerization of **1** to the chlorosubstituted vinyl alcohol, $CH_2{=}C(OH)Cl$ (**2**), and the prompt elimination of HCl from **2**. The branching ratio depends critically on the relative energies and vibrational frequencies of the respective rate-controlling transition states **1**/**3** and **1**/**2**.

• The transition structure **1**/**3** for the four-centered elimination of HCl from acetyl chloride is loose and highly asymmetric and would give rise to vibrationally excited HCl.

• A minor accessible reaction channel resulting in $CO + CH_3Cl$ has also been characterized. Decarbonylation will proceed preferably via the direct displacement channel over the addition−elimination mechanism.

Acknowledgment. We thank the Fund for Scientific Research (FWO-Vlaanderen) and KU Leuven (GOA) for financial support and the Laboratory of Quantum Chemistry for providing us with excellent computer facilities.

Supporting Information Available: Tables giving results of intrinsic reaction coordinate calculations (2 pages, print/PDF). See any current masthead page for ordering information and Web access instructions.

References and Notes

(1) Maricq, M. M.; Ball, J. C.; Straccia, A. M.; Szente, J. J. *Int. J. Chem. Kinet.* **1997**, *29*, 421.

(2) Manke, G. C.; Setser, D. W.; *J. Phys. Chem.* **1998**, *102*, 153; Maricq, M. M.; Szente, J. J. *Chem. Phys. Lett.* **1996**, *253*, 333; Scollard, D. J.; Treacy, J. J.; Sidebottom, H. W.; Balestra-Garcia, C.; Laverdet, G.; LeBras, G.; MacLeod, H.; Teton, S. *J. Phys. Chem.* **1993**, *97*, 4683; Mitchell, M. B.; Brunning, J.; Payne, W. A.; Stief, L. J. *J. Phys. Chem.* **1988**, *92*, 1502.

(3) Sumathi, R.; Chandra, A. K. *Chem. Phys.* **1994**, *181*, 73.

(4) Arunan, E.; Wategaonkar, S. J.; Setser, D. W. *J. Phys. Chem.* **1991**, *95*, 1539.

(5) Rowland, B.; Hess, W. P. *J. Phys. Chem. A* **1997**, *101*, 8049.

(6) Deshmukh, S.; Myers, J. D.; Xantheas, S. S.; Hess, W. P. *J. Phys. Chem.* **1994**, *98*, 12535.

(7) Berkowitz, J.; Ellison, G. B.; Gutman, D. *J. Phys. Chem.* **1994**, *98* 2744.

(8) *Handbook of Chemistry and Physics*, 75th ed.; CRC Press: Boca Raton, FL, 1995.

(9) Seakins, P. W.; Woodbridge, E. L.; Leone, S. R. *J. Phys. Chem.* **1993**, *97*, 5663.

(10) Sumathi, R.; Chandra, A. K. *J. Chem. Phys.* **1993**, *99*, 6531.

(11) Waschewsky, G. C. G.; Kash, P. W.; Myers, T. L.; Kitchen, D. C.; Butler, L. J. *J. Chem. Soc., Faraday Trans.* **1994**, *90*, 1582.

(12) Martin, X.; Moreno, M.; Lluch, J. M. *J. Phys. Chem.* **1993**, *97*, 12186.

(13) Martin, X.; Moreno, M.; Lluch, J. M. *J. Chem. Soc., Faraday Trans.* **1996**, *92*, 373.

(14) Frisch, M. J.; Trucks, G. W.; Head-Gordon, M.; Gill, P. M. W.; Wong, M. W.; Foresman, J. B.; Johnson, B. G.; Schlegel, H. B.; Robb, M. A.; Replogle, E. S.; Gomperts, R.; Andres, J. L.; Raghavachari, K.; Binkley, J. S.; Gonzalez, C.; Martin, R. J.; Fox, D. J.; Defrees, D. J.; Baker, J.; Stewart, J. J. P.; Pople, J. A. GAUSSIAN 94; Gaussian Inc.: Pittsburgh, PA, 1994.

(15) Gonzalez, C.; Schlegel, H. B. *J. Chem. Phys.* **1989**, *90*, 2154; Gonzalez, C.; Schlegel, H. B. *J. Phys. Chem.* **1990**, *94*, 5523.

(16) Arunan, E. *J. Phys. Chem.* **1997**, *101*, 4838.

(17) Srivatsava, A.; Arunan, E.; Manke, G., II; Setser, D. W.; Sumathi, R. *J. Phys. Chem. A* **1998**, *102*, 6412.

(18) Toto, J. L.; Pritchard, G. O.; Kirtman, B. *J. Phys. Chem.* **1994**, *98*, 8359.

(19) Nguyen, M. T.; Sengupta, D.; Raspoet, G.; Vanquickenborne, L. G. *J. Phys. Chem.* **1995**, *99*, 11883.

(20) Sumathi, R.; Nguyen, M. T. *J. Phys. Chem.* **1998**, *102*, 412.

(21) Sumathi, R.; Chandra, A. K. *Chem. Phys. Lett.* **1997**, *271*, 287.